Inhibiting Steel Corrosion in Simulated Concrete with Low Phosphate to Chloride Ratios

L. Yohai,[a] W. Schreiner,[b] M. B. Valcarce,[a] and M. Vázquez[a,*,z]

[a]*División Electroquímica Aplicada, Facultad de Ingeniería, UNMdP – INTEMA, CONICET, B7608FDQ Mar del Plata, Argentina*
[b]*Laboratório de Superfícies e Interfases, Departamento de Física, Universidade Federal do Paraná, 81531-990 Curitiba, Brazil*

Phosphate ions are studied as corrosion inhibitors in pore simulating solutions highly contaminated with chloride ions. The investigation aims at understanding the role of phosphates in the corrosion inhibition mechanism, employing potentiodynamic polarization tests, micro-Raman spectroscopy, impedance spectroscopy, X-ray photo electronic spectroscopy (XPS) and weight loss tests. Two inhibitor/chloride ratios were assessed, $[PO_4^{3-}]/[Cl^-] = 0.2$ and 0.6. When $[PO_4^{3-}]/[Cl^-] = 0.6$, pitting is inhibited, even after 90 days exposure. $[PO_4^{3-}]/[Cl^-] = 0.2$ only delayed the onset of localized attack. XPS showed that phosphates incorporate to the surface film. Phosphate ions behaved as mixed-type corrosion inhibitors. The results are interpreted by the participation of phosphates in the duplex passive film being formed on carbon steel.

Manuscript submitted June 16, 2016; revised manuscript received September 12, 2016. Published September 21, 2016.

The use of corrosion inhibitors has proven to be an efficient way to prevent rebars corrosion in concrete.[1–3] It is well-known that aggressive conditions, such as those associated to concrete carbonation or chloride ions contamination compromise the stability of the protective passive layer naturally formed on steel reinforcements.

Two approaches are generally used to study steel corrosion in concrete: using simulated pore solution or using actual concrete or mortar. The use of electrolytes that mimic pore solutions facilitates the control of the many parameters that influence rebar corrosion. This is the approach chosen in the present investigation.

For concrete, the most widely used corrosion inhibitor is calcium nitrite.[4–7] However, for ecological reasons, it needs to be replaced with less contaminant substances. In this sense, phosphate ions can be used as inhibiting agents as they are inexpensive and present low toxicity.

The performance of phosphate ions as inhibitors in simulated pore solutions has not been extensively studied.[8–13] The inhibition mechanism in alkaline solutions is still under discussion and a deeper understanding is needed to later evaluate its effectiveness in mortars or in concrete.

In a previous work, the effectiveness of a high dosage of sodium phosphate (0.3 mol L^{-1}) as corrosion inhibitor was tested in a pore simulating solution contaminated with chloride ions (0.3 mol L^{-1}, $[Cl^-]/[OH^-] = 3$, $[PO_4^{3-}]/[Cl^-] = 1$).[13] Also, a protection mechanism was proposed.[13] In this work, two dosages of sodium phosphate (0.1 and 0.3 mol L^{-1}) are compared in a synthetic medium (pH 13) that simulates the interstitial solution of concrete heavily contaminated with chloride ions (0.5 mol L^{-1} corresponding to $[Cl^-]/[OH^-] = 5$). The conditions chosen for this work include a lower phosphate-to-chloride ratio and a higher chloride contamination, as compared to the previous investigation. The lower dosage of inhibitor tested in this work (0.1 mol L^{-1}) has been selected in order to reduce costs and minimize changes in the mechanical properties associated to additives. The composition of the passive films is investigated to evaluate changes in the previously proposed protection mechanism that may result from this new phosphate dosage and chloride contamination levels.

Materials and Methods

Electrodes preparation.—The electrodes were constructed from construction steel. The main alloying elements are: Mn 0.635%, C 0.299%, Si 0.258% and Cu 0.227%.The rebars were cut into discs and included in acrylic resin, including an appropriated contact. The geometrical area exposed was 0.503 cm^2. The electrodes were abraded down to grade 1000 with emery paper and then rinsed with distilled water.

Electrolyte composition.—The electrolyte consisted of a pH 13 pore simulating solution (PSS) including KOH 0.08 mol L^{-1}, NaOH 0.02 mol L^{-1} and $Ca(OH)_2$ 0.001 mol L^{-1}. When chloride ions were incorporated, the Cl^- dosage used was 0.5 mol L^{-1} corresponding to $[Cl^-]/[OH^-] = 5$, (PSS + Cl^-). To evaluate the inhibitor, Na_3PO_4 was tested using two dosages: 0.1 and 0.3 mol L^{-1}, corresponding to $[PO_4^{3-}]/[Cl^-] = 0.2$ and 0.6 respectively. These solutions will be referred to as PSS + $[PO_4^{3-}]/[Cl^-] = 0.2$ and PSS + $[PO_4^{3-}]/[Cl^-] = 0.6$. All the experiments were carried out at room temperature ($20 \pm 2°C$).

Electrochemical evaluation.—The electrochemical experiments were carried out in stagnant solutions, using a three-electrode cell and a Gamry 600 or a Voltalab PGZ 100 potentiostat. As reference, a Hg/HgO electrode with 1 mol L^{-1} KOH solution (labeled as MOE, E = 0.123 V vs. NHE) was used. All the potentials are indicated against this electrode. The counter electrode was a platinum wire of large area.

The corrosion potential (E_{CORR}) was measured during 24 h. After two hours variations were negligible. All the electrochemical tests described below were carried out on electrodes kept 24 h at E_{CORR}.

Polarization resistance (R_P) was evaluated as $\Delta V/\Delta i$, from potential sweeps scanning ±0.015 V from the E_{CORR} at a scan rate of $1 \cdot 10^{-4}$ V s^{-1}.

For the electrochemical impedance spectroscopy (EIS) tests, the amplitude of the AC voltage signal was fixed at ±0.01 V_{rms} while the frequency varied between 20000 Hz and $1 \cdot 10^{-3}$ Hz. Figure 1 shows the equivalent circuits employed to analyze the data.[13] Circuit (a) has been used before to study oxide-coated metals[13–15] and circuit (b) to account for diffusion processes.[13,17] The data were fitted to the equivalent circuits using ZView.

To record anodic and cathodic polarization curves, the potentiodynamic scan started at the E_{CORR} and was swept at $1 \cdot 10^{-4}$ V s^{-1}. In the case of the anodic curves, the scan direction was inverted at 100 μA cm^{-2} after attaining a convenient degree of attack. The overall methodology complies with the recommendations of ASTM G61-86.[18]

Average values were calculated from at least five individual measurements in every one of the electrochemical evaluations described above.

*Electrochemical Society Member.
[z]E-mail: mvazquez@fi.mdp.edu.ar

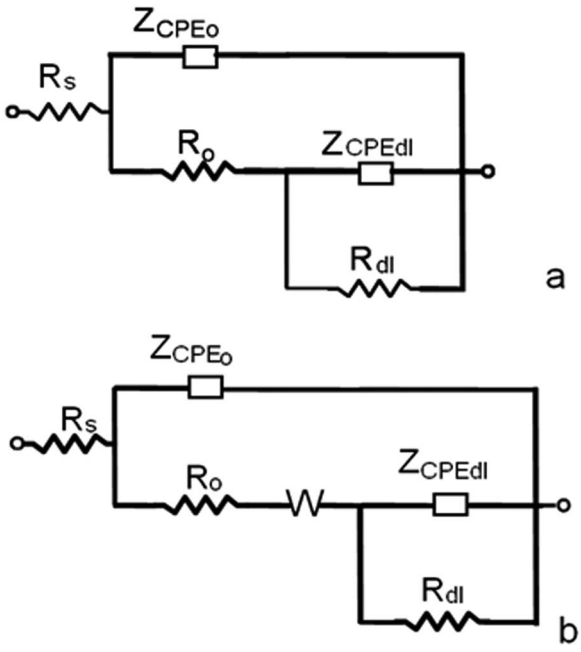

Figure 1. Equivalent circuits used to fit EIS results. Circuit (a) is typical of oxide-coated metals; circuit (b) presents an additional Warburg element, representing a diffusion process.

Weight loss determinations.—Weight loss tests were carried out following ASTM D 2688 Standard Test Methods for Corrosivity of Water in the Absence of Heat Transfer.[16] Discs were cut from the rebars and abraded with grade 120 emery paper. The area exposed was 5.67 cm^2. Weighted coupons were immersed for 90 days in PSS, PSS + Cl^-, PSS + $[PO_4^{3-}]/[Cl^-] = 0.2$ and PSS + $[PO_4^{3-}]/[Cl^-] = 0.6$. Each container held three coupons immersed at room temperature. One coupon removed from each container was dried under N_2 atmosphere and analyzed by Raman spectroscopy. The coupons were cleaned by immersion in HCl 1 mol L^{-1} and later neutralized with a saturated Na_2CO_3 solution, to be finally rinsed with distilled water, dried and weighted.

Surface analysis.—An Invia Reflex confocal Raman microprobe with Ar+ laser of 514 nm in backscattering mode was employed to register Raman spectra. The laser power was 25 mW and the laser spot had a diameter of 10 μm using a 50 × objective. There was no evident heating effect. An exposure time of 50 s and 3 accumulations were recorded. Raman spectra were taken after subjecting the electrodes to anodic polarization curves, on least five representative spots and were observed to be reproducible.

Thicker surface films were grown on carbon steel by immersing the samples during 8 days at E_{CORR}. After being withdrawn, the samples were dried under a steam of N_2. The XPS spectra were obtained using an XPS VG Microtech ESCA3000 (MgKα and AlKα radiations). The operating pressure was $3 \cdot 10^{-10}$ mbar. The angle between the analyzer axis and the sample surface normal was 45°. Survey spectra were recorded in the 0–1100 eV binding energy range, using 1 eV steps and a bandpass of 50 eV (not shown). The size of the steps and bandpass were reduced to 0.1 and 20 eV respectively, in order to conduct high resolution scans along regions of particular interest. Surface charging effects were compensated taking the binding energy (BE) of the C 1s line of residual carbon as reference (284.5 eV BE).[19] Complex XPS bands were analyzed using XI SDP32 software, version 4.3.

Results and Discussion

Corrosion potentials.—The corrosion potential (E_{CORR}) values were obtained after the 24 h immersion, as an average of not less than three independent measurements. In the case of PSS, a corrosion potential value around −208 ± 22 mV is typical of the passive state, as was discussed before.[13] As expected, the presence of Cl^- in the solution turns the potential more active close to −295 ± 75 mV. No significant differences were observed in the corrosion potential for solutions simultaneously containing chloride and phosphate ions (within experimental error). E_{CORR} values for PSS + $[PO_4^{3-}]/[Cl^-]$ = 0.2 and PSS + $[PO_4^{3-}]/[Cl^-] = 0.6$ were −319 ± 65 and −260 ± 64 mV, respectively. This behavior could be associated to the performance of mixed-type inhibitors.[13] This type of inhibitors influences both, the anodic and cathodic processes. Therefore in the presence of inhibitors, E_{CORR} should not be the only parameter used to investigate the tendency of steel to undergo corrosion.

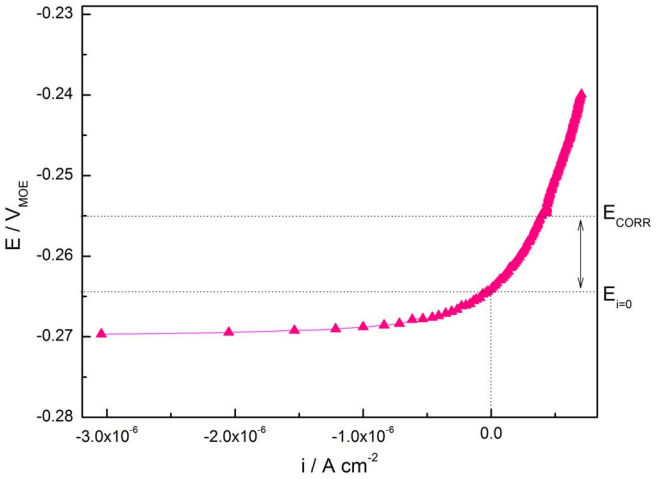

Figure 2. Polarization curve acquired by sweeping the potential ± 0.015 V from E_{CORR} in (▲) $[PO_4^{3-}]/[Cl^-] = 0.6$. Sweep rate: $1 \cdot 10^{-4}$ V s^{-1}.

Linear polarization resistance.—The most common way to determine Rp is by the linear polarization resistance method (LPR), scanning the potential ±0.015 V relative to the corrosion potential. The slope (dE/di) at zero-current potential corresponds to Rp. In the presence of chloride ions, Rp values around 22 ± 6 kΩ cm^2, are close to typical values of carbon steel in active dissolution (Rp lower than 10 kΩ cm^2).[20,21] In PSS as well as in solutions containing phosphates, the response is non-linear, as shown in Figure 2. The deviation from linearity can clearly be seen around i = 0. Furthermore, the potential at zero current does not match the corrosion potential. This type of behavior has been reported by many authors[20,22,23] and has been associated to limitations in the Stern and Geary methodology.[24] Gonzalez et al.[20] stated that the correct determination of the corrosion rate can be limited if Tafel slopes are unknown or vary with time, if values of the anodic and cathodic slopes are dissimilar and/or a long time is necessary to reach the steady state. Mansfeld et al.[25] established that linearity around i = 0 only occurs when Tafel slopes are equal (βa = βc). Mansfeld and Gonzalez[23,26] discussed that the linear polarization method is only valid in the absence of diffusion effects. In turn, Kouril et al.[22] concluded that the lack of linearity around i = 0 is a consequence of the inertia of passive systems to be polarized, even at low scan rates. To distinguish between active or passive state, these authors implemented a methodology based on the linear regression of the data. The coefficient of determination (R^2) was used as a tool to evaluate the deviation from linearity of the LPR curve compared to the ideal linear shape.[22] R^2 can be plotted against the difference between the zero current potential ($E_{i=0}$) and the corrosion potential (E_{CORR}). This difference ($E_{i=0}$ - E_{CORR}) characterizes an electrode's ability to be polarized. Figure 3 shows this representation for steel in the three chloride-containing solutions. As it can be seen, the points are separated into two different groups. Active surfaces are characterized by low values of ($E_{i=0}$ - E_{CORR}) and R^2 close to 1. This is the case

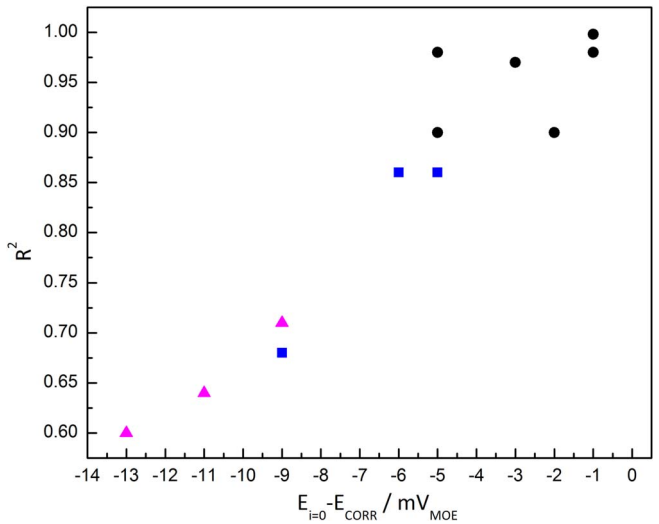

Figure 3. The coefficient of determination R^2 plotted against the difference between the zero current potential ($E_{i=0}$) and the corrosion potential (E_{CORR}) in (●) PSS + Cl^-; (■) $[PO_4^{3-}]/[Cl^-] = 0.2$; (▲) $[PO_4^{3-}]/[Cl^-] = 0.6$.

for steel immersed in PSS + Cl^-. In turn, passive surfaces are characterized by higher values of ($E_{i=0}$ - E_{CORR}) and lower R^2 values. This is the case for PSS + $[PO_4^{3-}]/[Cl^-] = 0.6$. An intermediate behavior was observed for PSS + $[PO_4^{3-}]/[Cl^-] = 0.2$. This analysis can then be useful to distinguish between active or passive surfaces as it has been shown before when studying the effectiveness of phosphates in solutions simulating carbonated concrete.[27]

Electrochemical impedance spectroscopy (EIS).—The results of the impedance spectra together with the fitting results for steel aged 24 h at E_{CORR} in PSS + Cl^-, PSS + $[PO_4^{3-}]/[Cl^-] = 0.2$ and PSS + $[PO_4^{3-}]/[Cl^-] = 0.6$ is show in Figure 4a using Nyquist representation. The fitting parameters for PSS + Cl^- and PSS + $[PO_4^{3-}]/[Cl^-] = 0.6$ are presented in Table I. In $[PO_4^{3-}]/[Cl^-] = 0.2$ the behavior is similar to that in PSS + $[PO_4^{3-}]/[Cl\text{-}] = 0.6$ (results not shown). R_s denotes the solution resistance, R_o the film resistance, Q_o the pseudo-capacitance of the surface film, Q_t the metal pseudo-capacitance, R_t the charge-transfer resistance for metal dissolution, and W a Warburg element associated to finite length diffusion.

Table I. Optimized parameters fitting data in Figure 4 to the equivalent circuits shown in Figure 1, calculated from at least five independent spectra.

	PSS + Cl^-	PSS + $[PO_4^{3-}]/[Cl^-] = 0.6$
$R_s/\Omega\ cm^2$	7.11	3.15
$Q_o/\mu\Omega^{-1}\ cm^{-2}s^n$	77.71	34.75
n_o	0.87	0.94
$R_o/k\Omega\ cm^2$	5.17	0.20
$W_R/\ k\Omega\ cm^2$	——	0.39
T/s	——	0.68
n_W	——	0.34
$Q_t/\mu\Omega^{-1}\ cm^{-2}\ s^n$	446.52	2156
n_t	0.62	0.68
$R_t/k\Omega\ cm^2$	35.69	73.03
% ξ	——	51.13

The constant phase element (Z_{CPE}) has been recurrently used in corroding electrodes. The impedance of this kind of elements is given by:

$$Z_{CPE} = [Q\,(j\omega)\,n]^{-1} \quad [1]$$

where Q is a constant with dimensions of $\Omega^{-1}\ cm^{-2}\ s^n$ and n a constant power, with $-1 < n < 1$. The imaginary component of the impedance can be represented as a function of frequency in logarithmic coordinates to quantify the CPE behavior.[28] As the imaginary part of the impedance is independent of the electrolyte resistance, the slope is constant in the whole frequency range. Thus, this plot allows the value of the n parameter to be obtained directly without fitting with equivalent circuits. As shown in Figure 4b, slopes of −0.90 and −0.87 were obtained with and without inhibitor respectively, in agreement with the n_0 values presented in Table I.

Warburg elements are frequently used to describe diffusion process along the pores in surface films. Finite length Warburg elements (Eq. 2 are typical of thin surface layers where low frequencies can penetrate the entire thickness and can be described by the following equation:

$$Z_w = \frac{W_R}{(iT\omega)^n} tanh\ (iT\omega)^n \quad [2]$$

where W_R is a parameter associated with solid phase diffusion and T is related to the effective diffusion coefficient (D) and the effective diffusion thickness (L) by $T = L^2/D$.[29]

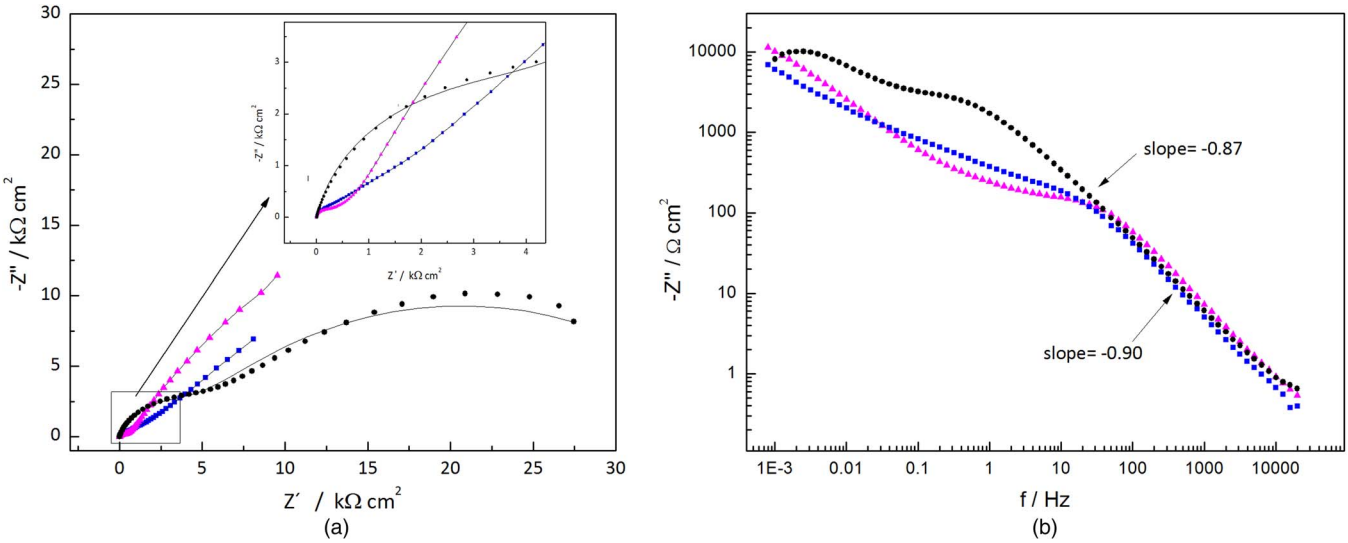

Figure 4. Impedance spectra and fit results for steel aged 24 h at E_{CORR} in (●) PSS + Cl^- and (▲) PSS + $[PO_4^{3-}]/[Cl^-] = 0.6$. (a) Nyquist representation and (b) imaginary part of impedance as function of frequency, in logarithmic scale.

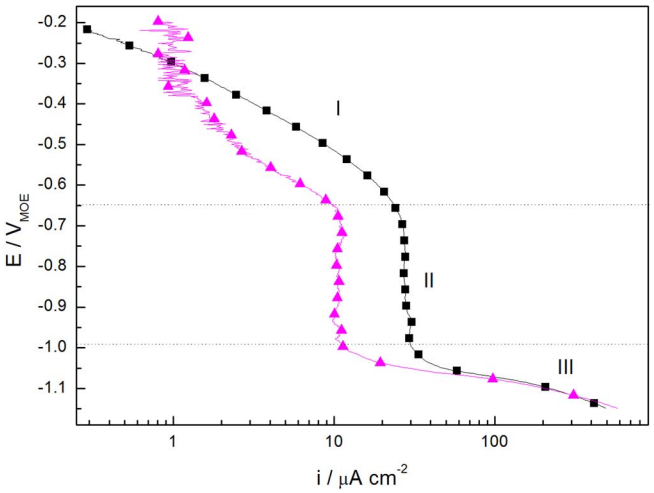

Figure 5. Cathodic polarization curves registered after keeping the electrodes for 24 h at the E_{CORR} in (●) PSS + Cl^- and (▲) PSS + $[PO_4^{3-}]/[Cl^-] = 0.6$.

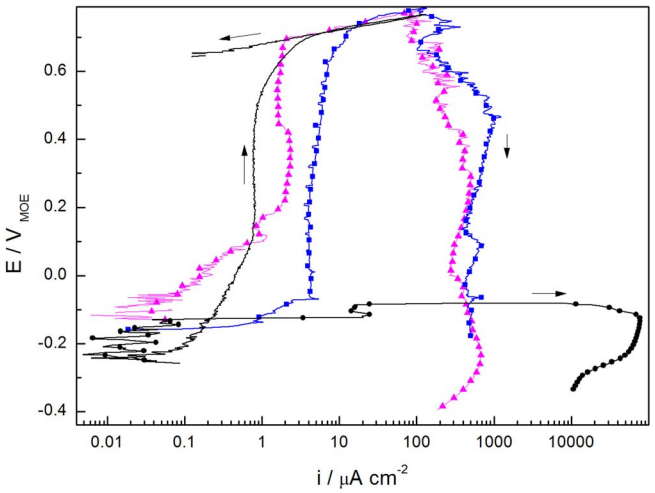

Figure 6. Anodic polarization curves registered after keeping the electrodes for 24 h at the E_{CORR} in (—) PSS, (●) PSS + Cl^-, (■) PSS + $[PO_4^{3-}]/[Cl^-] = 0.2$ and (▲) PSS + $[PO_4^{3-}]/[Cl^-] = 0.6$.

The results for steel in PSS + Cl^- can be interpreted using two time constants. This response indicates the development of a surface layer. The same behavior had been observed earlier with a lower chloride content (0.3 mol L^{-1} Cl^-).[13] In comparison with our previous results, an increase of chloride ions content in solution leads to higher values of Q_o and lower n_o, indicating the development of a poorly protective layer. Besides, the oxide resistance is an order of magnitude lower. A decrease in R_t together with higher values of Q_t can also be observed. R_t values for PSS + Cl^- are similar to the ones obtained by linear polarization.

When phosphates are present in the solution, Q_o decreases when compared to an inhibitor-free electrolyte and n_o increases to values higher than 0.9 (Table I). Q_o values close to 50 $\mu\Omega^{-1}$ $cm^{-2}s^n$ and n_o values greater than 0.9 can be related to the presence of a protective layer.[7,21,30] R_o changes substantially when comparing PSS + Cl^- to $[PO_4^{3-}]/[Cl^-] = 0.6$. This behavior was also found in $[PO_4^{3-}]/[Cl^-] = 0.2$ and $[PO_4^{3-}]/[Cl^-] = 1$ and attributed to changes in the composition of the passive layer which impact the electronic properties of the passive layers.[13] Moreover, Q_t values are too big to be associated with a double layer capacitance, so that they can be attributed to diffusion impedance combined with a charge transfer process.[8,13] The diffusion process is most likely due to oxygen transport through a non-conducting layer. Diffusion can also be attributed to a more difficult movement of cation vacancies. The increment in R_t values in the presence of the inhibitor may also be due to changes in the film composition as well as to the diffusion of oxygen and/or cation vacancies.[30] The percentage of inhibition shown in Table I was calculated as:

$$\%\zeta = \left[1 - \frac{Rt_{\text{without inhibitor}}}{Rt_{\text{with inhibitor}}}\right] x100 \qquad [3]$$

Polarization curves.—Cathodic polarization curves for steel in PSS + Cl^- and PSS + $[PO_4^{3-}]/[Cl^-] = 0.6$ after 24 h at the E_{CORR} are shown in Figure 5. Three different sectors can be observed. Region I, between E_{CORR} and −0.65 V, where reduction processes occur under mixed control (diffusion + activation); region II, between −0.65 V and −1 V, where oxygen diffusion to the metal/film interface controls the current and region III, from −1 V, where the current is controlled by activation and associated to H_2O decomposition.[31] The limiting current for oxygen diffusion in PSS + Cl^- is three times higher than for PSS + $[PO_4^{3-}]/[Cl^-] = 0.6$, suggesting the presence of a more compact and dense surface film when the inhibitor is present, which influences and limits oxygen diffusion.

Figure 6 shows the anodic polarization curves registered after keeping the electrodes for 24 h at the E_{CORR} in PSS + Cl^-, PSS + $[PO_4^{3-}]/[Cl^-] = 0.2$ and PSS + $[PO_4^{3-}]/[Cl^-] = 0.6$. The curve in PSS, where steel remains passive, has been shown in our previous work and added here for comparison.[13] In the presence of chloride ions, pitting occurred at potentials around −0.05 V_{MOE}. Chloride ions play a key role on the passivity breakdown of steel as a result of the competition between the stabilization of the surface film by OH^- adsorption and the rupture of the film by Cl^- adsorption. When chloride ions become more active than hydroxyl ions, pitting starts.[7,32] In the presence of phosphate ions, pitting was not completely inhibited but very much delayed, starting around 0.6 V_{MOE}. Average values for the pitting potential (E_{PIT}), for the corrosion potential (E_{CORR}) and for the difference (E_{PIT}-E_{CORR}) from at least five independent experiments are shown in Table II. The i_{PAS} measured for steel in PSS + $[PO_4^{3-}]/[Cl^-] = 0.6$ decreases five times when compared to PSS + Cl^- and nearly reduces to half for steel in PSS + $[PO_4^{3-}]/[Cl^-] = 0.2$. Despite the fact that pitting is not inhibited, the difference (E_{PIT}-E_{CORR}) increases markedly in presence of phosphates, which can be interpreted as a better resistance to pitting. Repassivation of the surfaces was not observed in any case.

Images of the electrodes after having performed the anodic polarization curves are shown in Figure 7. In the absence of inhibitor the surface appears heavily attacked with small pits over the entire surface with high quantities of reddish corrosion products. In contrast, when the inhibitor is present, the attack is localized with pits occupying a fraction of the electrode surface. The density of pits decreases when the inhibitor content increases.

Table II. Electrochemical parameters obtained from at least five anodic polarization curves for steel in the conditions evaluated.

	E_{CORR} /V	E_{PIT} /V	E_{PIT}-E_{CORR} /V	i_{PAS} /μA cm^{-2}
PSS	−0.208 ± 0.022	—-	—-	0.7 ± 0.1
PSS + Cl^-	−0.295 ± 75	−0.048 ± 0.102	0.159 ± 0.095	8.2 ± 6
PSS + $[PO_4^{3-}]/[Cl^-] = 0.2$	−0.319 ± 0.065	0.574 ±0.033	0.870 ± 0.034	4.6 ± 2.2
PSS + $[PO_4^{3-}]/[Cl^-] = 0.6$	−0.260 ± 0.064	0.610 ± 0.113	0.841 ± 0.055	1.6 ± 0.2

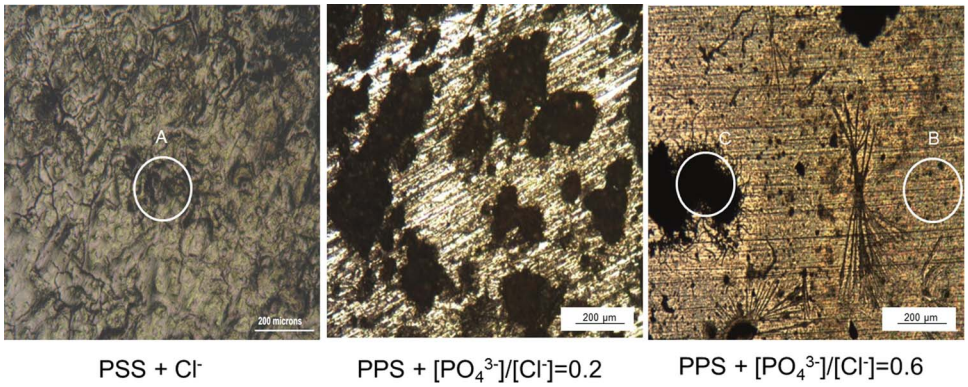

Figure 7. Images of the electrodes after carrying out the anodic polarization curves. A, B and C refer to the Raman spectra in Figure 10.

Table III. Weight loss results for coupons immersed during 90 days at E_{CORR}.

	Weight loss (mg)	Attack	i_{CORR}/µA cm^{-2}	% ξ
PSS	0.1	none	0.008	-
PSS + Cl^-	300.8	pitting	23.6	-
PSS + $[PO_4^{3-}]/[Cl^-] = 0.6$	4.1	none	0.3	98.6
PSS + $[PO_4^{3-}]/[Cl^-] = 0.2$	129.2	pitting	10.1	57.0

Weight loss tests.—The inhibitor efficiency was also evaluated during prolonged immersion periods of time. Ninety days weight-loss tests were carried out as described in detail in Electrolyte composition section. The corrosion current density (i_{CORR}) is calculated using Faraday's law (Eq. 3) and presented in Table III.

$$i_{CORR} = \frac{m\ F}{A\ t\ eq} \quad [4]$$

where A is the geometrical area, m is the mass lost, F is the Faraday constant, t is the exposure time and eq is the equivalent weight (Fe eq = 27.92 g/mol). Figure 8 shows photographs of the coupons after 90 days of immersion in each electrolyte. An important degree of attack is evident on the coupons immersed in PSS + Cl^- and in PSS + $[PO_4^{3-}]/[Cl^-] = 0.2$. When using the lower dosage of phosphate ions, a decrease in the i_{CORR} value is observed, but the risk of localized attack could not be neglected. However, no attack was detected in the case of coupons immersed in PSS + $[PO_4^{3-}]/[Cl^-] = 0.6$. Also, the i_{CORR} values are typical of the passive state, even when the samples have been immersed during 90 days. The percentages of inhibition shown in Table III were calculated assuming uniform corrosion in all the conditions tested by means of the following equation

$$\%\zeta = \left[1 - \frac{i_{\text{corr with inhibitor}}}{i_{\text{corr without inhibitor}}}\right] x\,100 \quad [5]$$

Immersion in PSS is taken as the blank situation, where corrosion and weight loss are insignificant and i_{CORR} values are typical of passive steel. It can be seen that the inhibition efficiency increases markedly for the higher phosphate dosage, attaining a very satisfactory value close to 99%, where no visible evidence of localized attack was detected. These inhibition efficiency values are higher than those obtained by EIS. Most likely, values obtained by weight loss after a 90 days immersion are more realistic than those obtained only after 24 h of immersion.

Raman confocal spectroscopy.—Ex situ Raman spectra were registered in order to characterize the passive films and the corrosion products after inducing the pitting process by anodic polarization and weight loss. The results should be interpreted with caution because for this technique a relatively high laser power needs to be used. This is so because the most frequent iron oxides and oxyhydroxides are poor light scatters. When performing these experiments, precautions were taken so as not to induce chemical changes by laser heating. Figure 7 shows images of the steel surfaces after having registered anodic polarization curves in PSS + Cl^- and PSS + $[PO_4^{3-}]/[Cl^-]$ = 0.6. The circles in Figure 7 point to the regions where Raman spectra were collected (zone A in PSS + Cl^- and; zones C and B in PSS + $[PO_4^{3-}]/[Cl^-] = 0.6$, with and without corrosion products respectively). The corresponding Raman spectra are presented in Figure 9 and have been labelled accordingly. Bands at 220 cm^{-1}, 280 cm^{-1}, 395 cm^{-1} and 595 cm^{-1} in spectrum A are typical of α-FeOOH and/or α-Fe_2O_3. The band at 245 cm^{-1} can be associated to γ-FeOOH. The signal at 680 cm^{-1} is typical of Fe_3O_4.[33–35] In spectrum C the same bands attributed to iron oxides/oxohydroxides can be observed. Also, three bands between 930 and 1100 cm^{-1} appear which could be

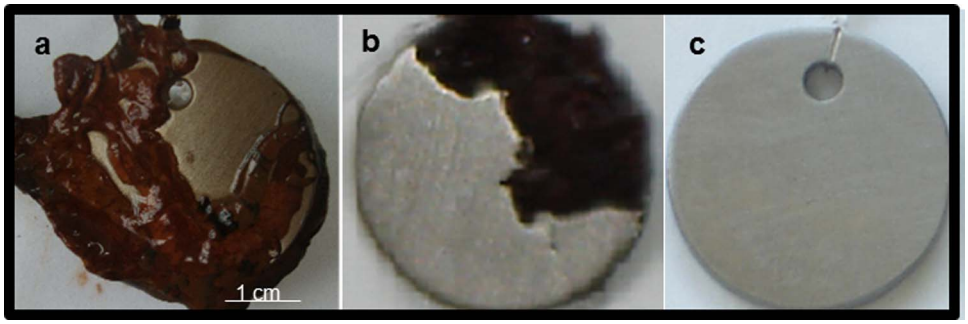

Figure 8. Photographs of the coupons after 90 days of immersion in each electrolyte at E_{CORR}. a) PSS + Cl^-; b) PSS + $[PO_4^{3-}]/[Cl^-] = 0.2$ and c) PSS + $[PO_4^{3-}]/[Cl^-] = 0.6$.

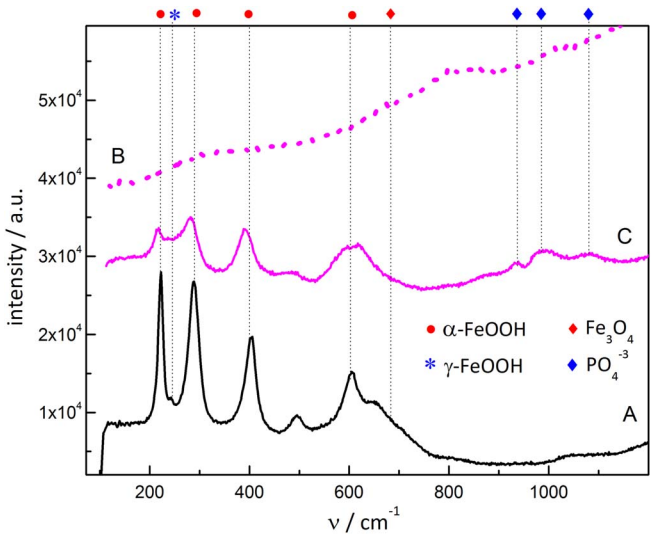

Figure 9. Raman spectra recorded on electrodes subjected to anodic polarization curves in (A) PSS + Cl^- and PSS + $[PO_4^{3-}]/[Cl^-] = 0.6$, with (C) and without (B) corrosion products.

attributed to the incorporation of phosphates into the corrosion products. Phosphate ions are known to have four active Raman bands: a strong one at 935 cm^{-1} due to P-O symmetric stretch together with three weak ones at 1007 cm^{-1} (P-O antisymmetric) and 550 and 412 cm^{-1} (deformation). Another band at 1081 cm^{-1} can be related to an antisymmetric stretching mode of hydrogen phosphate.[36] Spectrum B corresponds to a region away from the pits. There is no evidence of defined bands in this spectrum. The absence of typical signals may be due to the presence of a very thin passive film on the steel surface. Also, iron oxides or oxohydroxides could be present as an amorphous or disordered structure, obstructing a clear identification.[34]

The Raman spectra of the corrosion products on the weight-loss coupons in PSS + Cl^- and PSS + $[PO_4^{3-}]/[Cl^-] = 0.2$ are presented in Figure 10. The results obtained after 90 days are in agreement with those presented in Figure 9, which were recorded after performing the anodic polarization curves. In the case of PSS + Cl^-, bands associated to α-FeOOH and/or α-Fe_2O_3 are present in the corrosion products. In PSS + $[PO_4^{3-}]/[Cl^-] = 0.2$ the incorporation of phosphate ions to the corrosion products is evident. Furthermore, the Raman spectra of the coupon passivated in $[PO_4^{3-}]/[Cl^-] = 0.6$ was included in Figure 10. In the presence of the inhibitor, the intensity of the signal is low and there are no well-defined bands, in agreement with the results presented before (see Figure 9).

X-ray photoelectronic spectroscopy (XPS).—XPS spectra were recorded on samples kept for 192 h immersed in each solution. In every case, peak C1s (**B.E.**: 284.5 eV) was taken as reference to correct the binding energy of the rest of the peaks. Figure 11 presents the results for the surface films grown in PSS + Cl^- and PSS + $[PO_4^{3-}]/[Cl^-] = 0.6$, where peaks corresponding to $Fe2p_{3/2}$ and O1s are shown. For PSS + $[PO_4^{3-}]/[Cl^-] = 0.6$ the peak P2p was also included in Figure 11. Similar results were obtained for steel in contact with in $[PO_4^{3-}]/[Cl^-] = 0.2$ and $[PO_4^{3-}]/[Cl^-] = 0.6$. The parameters obtained from deconvoluting the different signals are summarized in Table IV. In the presence of the inhibitor, the $Fe2p_{3/2}$ peak includes contributions from Fe^0, Fe(II) and Fe(III).[37,38] However, in PSS + Cl^- the spectrum becomes noisy and poorly defined. This can be associated to the presence of a highly porous passive film.[37] In this case, there is no contribution from the Fe^0 peak, suggesting that the thickness of the surface film is higher than 10 nm (as this is the maximum depth that can be evaluated by XPS).[30] In contrast, when the inhibitor is present, the Fe^0 peak is present, which suggests a thinner film compared to PSS + Cl^-. Table V shows Fe^{III}/Fe^{II} and Fe^{OX}/Fe^{M} ratios, calculated from the analysis of XPS peaks. Fe^{OX}/Fe^{M} describes the amount of Fe(II) and Fe(III) oxides formed, relative to the amount of Fe^0 (metallic iron, Fe^M). Fe^{OX} is estimated by adding the contribution from Fe(II) and Fe(III) peaks in Table IV.[37] The Fe^{OX}/Fe^{M} ratios for $[PO_4^{3-}]/[Cl^-] = 0.2$ and $[PO_4^{3-}]/[Cl^-] = 0.6$ are lower than PSS + Cl^-, indicating that the amount of corrosion products being formed is similar in the presence of the inhibitor. However, the Fe^{III}/Fe^{II} ratio reaches a maximum for PSS + Cl^-, and decreases when the inhibitor concentration increases. The increment of Fe(II) compounds in the passive film can be associated to a better corrosion resistance.

As regards the O1s peak, the two inhibitor dosages present contributions from O^{-2}, OH^- and PO_4^{3-}. No difference in the amount of PO_4^{-3} was found between $[PO_4^{-3}]/[Cl^-] = 0.2$ and $[PO_4^{-3}]/[Cl^-] = 0.6$, where roughly 5% of the O1s signal comes from PO_4^{-3}. In turn, peak P2p (B.E.: 132.5 eV) confirms that phosphorus is incorporated as phosphate (see inset Figure 11).

The Fe^{OX}/Fe^{M} ratio could be used to calculate the film oxide thickness assuming a uniform iron oxide layer present on the entire surface. Accordingly, the thickness of the surface film (d_{ox}) can be calculated

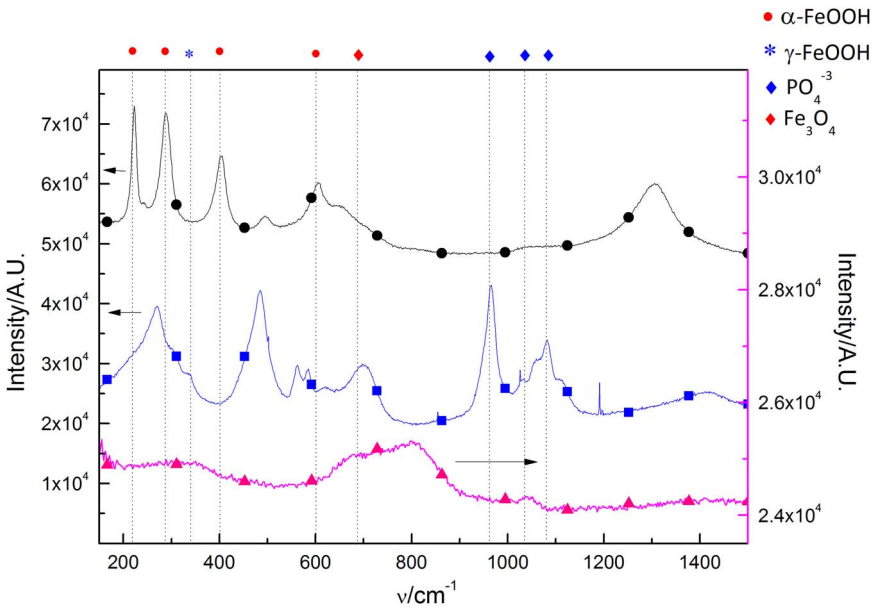

Figure 10. Raman spectra recorded on corrosion products in (●) PSS + Cl^- and (■) $[PO_4^{3-}]/[Cl^-] = 0.2$; and on passive film in PSS + $[PO_4^{3-}]/[Cl^-] = 0.6$. Coupons were immersed for 90 days in each electrolyte at E_{CORR}.

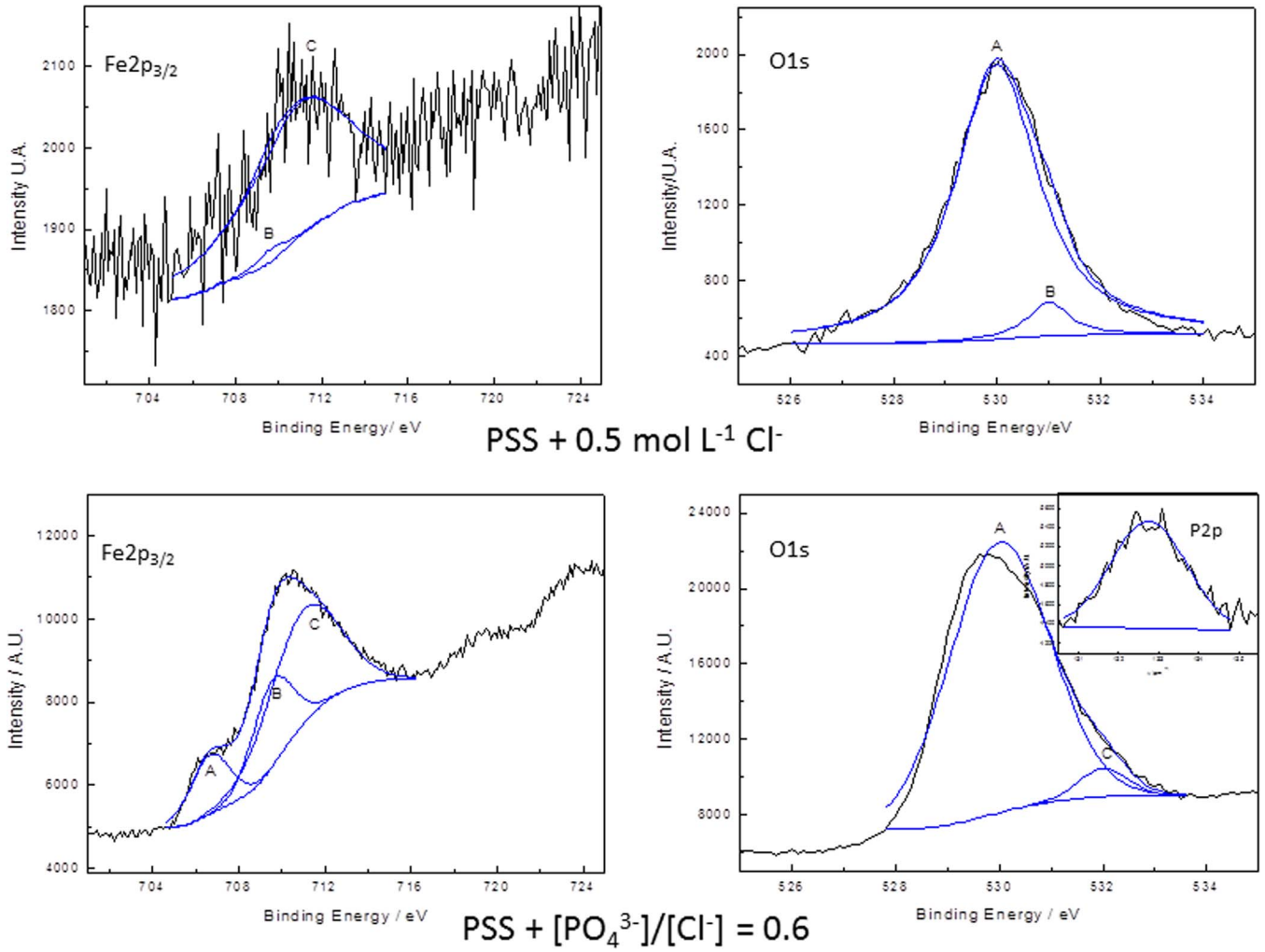

Figure 11. XPS spectra for passive films grown on steel for 192 h at E_{CORR} in PSS + Cl^-, PSS + $[PO_4^{3-}]/[Cl^-] = 0.6$.

Table IV. Characteristic parameters associated to the elements present in the surface film.

Condition	Peak	Compound		Binding Energy/eV	FWHM/eV	Atomic composition %
SAA + 0.5 mol L^{-1} Cl^-	Fe2p3/2	Fe0	A	706.7	—	—
		Fe(II)	B	709.6	1.5	2.4
		Fe(III)	C	711	5.9	97.6
	O1s	O^{-2}	A	530	1.9	94.3
		OH^-	B	531	0.9	5.7
SAA + $[PO_4^{3-}]/[Cl^-] = 0.2$	$Fe2p_{3/2}$	Fe^0	A	706.7	2.2	19.9
		Fe(II)	B	709.6	2.3	12.7
		Fe(III)	C	711	3.9	67.4
	O1s	O^{-2}	A	530	2.2	87
		OH^-	B	531	1.2	7.9
		PO_4^{3-}	C	532	1.1	5.2
SAA + $[PO_4^{3-}]/[Cl^-] = 0.6$	$Fe2p_{3/2}$	Fe^0	A	706.7	2.2	16.8
		Fe(II)	B	709.6	2.2	25
		Fe(III)	C	711	3.9	58.2
	O1s	O^{-2}	A	530	2.3	94.9
		OH^-	B	531	2.5	0.1
		PO_4^{3-}	C	532	1.1	5.1

Table V. Fe^{III}/Fe^{II} and Fe^{OX}/Fe^{M} ratios, calculated from the analysis of XPS peaks.

Condition	Fe^{III}/Fe^{II}	Fe^{OX}/Fe^{M}	d_{ox}(nm)
PSS + 0.5 mol L^{-1} Cl^-	40.7	High	>10
PSS + $[PO_4^{3-}]/[Cl^-] = 0.2$	5.3	4.0	5.5
PSS + $[PO_4^{3-}]/[Cl^-] = 0.6$	2.3	4.9	5.4

as:[39]

$$d_{ox} = \lambda_{ox}^{Fe} \cos\theta \ln\left(1 + \frac{I_{ox}^{Fe}}{I_M^{Fe}} \cdot \frac{N_M^{Fe}}{N_{ox}^{Fe}} \cdot \frac{\lambda_M^{Fe}}{\lambda_{ox}^{Fe}}\right) \quad [6]$$

where θ is the refracted angle to the normal surface; and I_{ox}^{Fe} and I_M^{Fe} correspond to the intensity of the peaks related to oxides and to iron, respectively. N_M^{Fe} and N_{ox}^{Fe} are atom densities of iron oxide and metallic iron (N_M^{Fe}= 38 atom/nm^3 and N_{ox}^{Fe}= 84 atom/nm^3 respectively). In turn, λ_M^{Fe} and λ_{ox}^{Fe} are the attenuation lengths of iron oxide and iron, which can be calculated as:[39]

$$\lambda_{ox}^{Fe} = 0.72\,(a_{ox})^{3/2}(E_k)^{1/2} \quad [7]$$

$$\lambda_M^{Fe} = 0.41\,(a_M)^{3/2}(E_k)^{1/2} \quad [8]$$

where E_k (eV) is the kinetic energy of iron (779 eV); a_{ox} and a_M (nm) are the monolayer thicknesses of iron oxide and metallic iron, respectively

$$a_{ox} = \left(\frac{1}{N_{ox}^{Fe}}\right)^{1/3} \quad [9]$$

$$a_M = \left(\frac{1}{N_M^{Fe}}\right)^{1/3} \quad [10]$$

Using Eqs. 6–10, the oxide film thicknesses was calculated for those conditions where the inhibitor was present. The results are presented in Table V. The film thickness decreases in the presence of inhibitor but is similar for the two inhibitor dosages tested.

Inhibition mechanism.—As proposed in our previous publication,[13] a passive layer comprising an inner layer of Fe_3O_4 and an outer layer of FeOOH develops at E_{CORR} on carbon steel immersed in aerated PSS + Cl^-. As immersion time increases, the ratio Fe^{III}/Fe^{II} increases toward the interior, creating cation vacancies and increasing stress in the surface film. This process is faster in the presence of chloride ions.

In a previous work[13] a protection mechanism has been proposed when phosphate ions are present. The presence of inhibitor in the system may cause the precipitation of ferrous phosphate by a dissolution-precipitation mechanism:

$$3Fe + 2PO_4^{-3} \rightarrow (Fe)_3(PO_4)_2 + 6e^- \quad [11]$$

Below this phosphate layer, a protective passive film of Fe_3O_4 could be developed via a solid-state process. The most external $(Fe)_3(PO_4)_2$ could gradually be oxidized to $FePO_4$ by reaction with oxygen, delaying oxygen diffusion through the duplex surface layer. This layer could behave as a barrier, preventing Fe_3O_4 oxidation and deferring the attack by chloride ions. Fe_3O_4 is known to inhibit iron dissolution. In PSS + $[PO_4^{3-}]/[Cl^-] = 0.6$, the proposed mechanism could be applied. However, low phosphate concentrations might not be sufficient to consolidate the barrier layer, decreasing the overall inhibition efficiency.

Conclusions

The performance of phosphate ions as inhibiting agent has been investigated using simulating solutions that mimic the composition of chloride-contaminated concrete pores.

Phosphate ions have no effect on the corrosion potential but influence both, the cathodic and anodic branches of the corrosion process, behaving as a mixed-type inhibitor.

The presence of 0.5 mol L^{-1} chloride ions changes the composition of the surface film and promotes localized corrosion. Pits appear after anodic polarization or after long immersion periods at E_{CORR}. When phosphate ions are incorporated, pitting resistance improves and (E_{PIT} – E_{CORR}) increases, although there is no evidence of repassivation. For the highest inhibitor content ($[PO_4^{3-}]/[Cl^-] = 0.6$) pitting is inhibited even after 90 days at E_{CORR}, with minimal weight loss and an inhibition efficiency greater than 98%. The lowest inhibitor content ($[PO_4^{3-}]/[Cl^-] = 0.2$) was not enough to prevent pitting, at least for this high chloride concentration.

The composition of the surface layer changes when phosphates are incorporated to the electrolyte as suggested by EIS results. In this case (PSS + Cl^- + PO_4^{-3}) a duplex film is likely to be formed: an outer thin layer of ferrous and ferric phosphate and an inner, protective layer of Fe_3O_4 formed via a solid-state process. The outer phosphate layer could delay oxygen diffusion, hindering further oxidation at the metal-film interface. This duplex layer is more protective when $[PO_4^{3-}]/[Cl^-] = 0.6$ as shown by LPR, EIS and weight loss tests, exhibiting lower passive currents and better resistance to pitting attack. The role played by phosphates in the corrosion inhibition mechanism was finally explained by their incorporation to the surface film (confirmed by XPS).

Acknowledgments

This work has been supported by the University of Mar del Plata (grant 15/G391), as well as by the National Research Council (CONICET, PIP0670). L. Yohai wishes to thank CONICET, Argentina, for her fellowship.

References

1. B. Elsener, *Corrosion inhibitors for steel in concrete. State of the art report*, Maney Publishing, London (2001).
2. J. M. Gaidis, *Cem. Concr. Compos.*, **26**, 181 (2004).
3. C. M. Hansson, L. Mammoliti, and B. B. Hope, *Cem. Con. Res.*, **28**, 1775 (1998).
4. K. Y. Ann, H. S. Jung, H. S. Kim, S. S. Kim, and H. Y. Moon, *Cem. Con. Res.*, **36**, 530 (2006).
5. N. S. Berke and M. C. Hicks, *Cem. Concr. Compos.*, **26**, 191 (2004).
6. V. T. Ngala, C. L. Page, and M. M. Page, *Corros. Sci.*, **44**, 2073 (2002).
7. M. B. Valcarce and M. Vázquez, *Electrochim. Acta*, **53**, 5007 (2008).
8. L. Dhouibi, E. Triki, M. Salta, P. Rodrigues, and A. Raharinaivo, *Materials and Structures*, **36**(8), 530 (2003).
9. N. Etteyeb, L. Dhouibi, M. Sanchez, C. Alonso, C. Andrade, and E. Triki, *J. Mater. Sci.*, **42**, 4721 (2007).
10. J. M. R. Génin, L. Dhouibi, P. Refait, M. Abdelmoula, and E. Triki, *Corrosion*, **58**, 467 (2002).
11. H. Nahali, L. Dhouibi, and H. Idrissi, *Construction and Building Materials*, **50**, 87 (2014).
12. M. Reffass, R. Sabot, M. Jeannin, C. Berziou, and P. Refait, *Electrochim. Acta*, **54**, 4389 (2009).
13. L. Yohai, M. Vázquez, and M. B. Valcarce, *Electrochim. Acta*, **102**, 88 (2013).
14. M. B. Valcarce and M. Vázquez, *Mater. Chem. Phys.*, **115**, 313 (2009).
15. A. Palit and S. O. Pehkonen, *Corrosion Science*, **42**, 1801 (2000).
16. *American Society of Testing and Materials*, ASTM D2688, Philadelphia, 1993.
17. C. Liu, Q. Bi, A. Leyland, and A. Matthews, *Corrosion Science*, **45**, 1257 (2003).
18. *American Society of Testing and Materials*, ASTM G61-86, Philadelphia, 1993.
19. J. F. Moulder, W. F. Stickle, P. E. Sobol, and K. D. Bomben, *Handbook of X-ray photoelectron spectroscopy*, Physical Electronics Inc., Minnesota, 1995.
20. J. A. González, J. M. Miranda, N. Birbilis, and S. Feliu, *Corrosion*, **61**, 37 (2005).
21. M. B. Valcarce, C. López, and M. Vázquez, *Journal of the Electrochemical Society*, **159**, C244 (2012).
22. M. Kouřil, P. Novák, and M. Bojko, *Cem Concr Compos*, **28**, 220 (2006).
23. F. Mansfeld, *Corrosion (Houston)*, **61**, 739 (2005).
24. M. Stern and A. L. Geary, *J. Electrochem. Soc.*, **104**, 56 (1957).
25. F. Mansfeld, *Advances in corrosion science and technology*, **6**, 163 (1976).
26. J. A. Gonzalez, J. M. Miranda, and N. Birbilis, *Corrosion (Houston)*, **61**, 741 (2005).
27. L. Yohai, W. H. Schreiner, M. Vázquez, and M. B. Valcarce, *Electrochim. Acta*, **202**, 231 (2015).
28. J. B. Jorcin, M. E. Orazem, N. Pébère, and B. Tribollet, *Electrochimica Acta*, **51**, 1473 (2006).
29. ZPlot for Windows Scribner Associates Inc., 1998.

30. W. Xu, K. Daub, X. Zhang, J. J. Noel, D. W. Shoesmith, and J. C. Wren, *Electrochim. Acta*, **54**, 5727 (2009).
31. N. Etteyeb, L. Dhouibi, H. Takenouti, M. C. Alonso, and E. Triki, *Electrochim. Acta*, **52**, 7506 (2007).
32. F. Foulkes and P. McGrath, *Cem. and Conc. Res.*, **29**, 873 (1999).
33. A. Hugot-Le Goff, J. Flis, N. Boucherit, S. Joiret, and J. Wilinski, *J. Electrochem. Soc.*, **137**, 2684 (1990).
34. B. DıÉaz, S. Joiret, M. Keddam, X. R. Nóvoa, M. C. Pérez, and H. Takenouti, *Electrochimica Acta*, **49**, 3039 (2004).
35. F. Dubois, C. Mendibide, T. Pagnier, F. Perrard, and C. Duret, *Corrosion Science*, **50**, 3401 (2008).
36. S. Simard, M. Odziemkowski, D. E. Irish, L. Brossard, and H. Ménard, *Journal of Applied Electrochemistry*, **31**, 913 (2001).
37. P. Ghods, O. B. Isgor, J. R. Brown, F. Bensebaa, and D. Kingston, *Applied Surface Science*, **257**, 4669 (2011).
38. L. Q. Guo, M. C. Lin, L. J. Qiao, and A. A. Volinsky, *Corrosion Science*, **78**, 55 (2014).
39. M. P. Seah and W. A. Dench, *Surface and Interface Analysis*, **1**, 2 (1979).